

An Ab Initio Molecular Orbital–Valence Bond (MOVB) Method for Simulating Chemical Reactions in Solution

Yirong Mo[†] and Jiali Gao^{*,†}

Department of Chemistry and Center for Computational Research, State University of New York at Buffalo, Buffalo, New York 14260

Received: November 16, 1999; In Final Form: January 27, 2000

A mixed molecular orbital and valence bond (MOVB) method for describing the potential energy surface of reactive systems has been developed and applied to a model proton transfer reaction in aqueous solution. The MOVB method is based on a block-localized wave function (BLW) approach for defining the diabatic electronic states. Then, a configuration interaction Hamiltonian is constructed using these diabatic states as the basis function. It was found that the electronic coupling energy is large with a value of about 30 kcal/mol for the $\text{H}_3\text{N}-\text{H}-\text{NH}_3^+$ system, whereas the predicted activation barrier is only 1.2 kcal/mol using the 3-21G basis set. The MOVB results are found to be in good accord with the corresponding ab initio Hartree–Fock calculations for the proton transfer process. We have also incorporated solvent effects into the MOVB Hamiltonian in the spirit of combined QM/MM calculations, and have modeled the proton transfer between ammonium ion and ammonia in water using Monte Carlo simulations. The potential of mean force was computed via free energy perturbation coupled with umbrella sampling techniques using (1) an energy gap mapping approach, and (2) a geometrical mapping procedure. Solvent effects increase the barrier height by about 2.2 kcal/mol from the MOVB and HF ground state potential energy surface. The present study demonstrated the feasibility of ab initio MOVB method for studying chemical reactions by incorporating explicit solvent effects in the description of the reaction coordinate in combined QM/MM simulations.

1. Introduction

Quantum mechanical calculations of reaction rates in solution represent a great challenge in theoretical chemistry because of the complexity and the large number of molecules involved in the system. Furthermore, the traditional approach of transition structure determination and reaction path following,^{1–5} typically used for gas-phase reactions, is complicated by the need for specific consideration of the fluctuations of the collective solvent coordinates accompanying the chemical transformation.^{6,7} Practical procedures have been established to circumvent the first problem by partitioning the condensed-phase system into a reactive region that is treated quantum mechanically (QM) and a bath region consisting of the rest of the system that is approximated by molecular mechanics (MM).^{8–13} Such a combined QM/MM approach takes advantage of the accuracy offered by quantum chemical models for chemical reactivity and computational efficiency of the MM force field. Importantly, the method can be systematically improved by either increasing the level of theory in the QM model or enhancing the classical representation of the solvent.¹⁴ Numerous studies have demonstrated a wide range of applications of combined QM/MM methods, including chemical reactions in solution and enzymes and solvent effects on electronic excited states.^{8–21}

To determine a reaction rate in solution, it is necessary to obtain the free energy of activation in solution. The prerequisite for such calculations is a reliable and general description of the potential energy surface (PES) for the reactive system that undergoes bond breaking and formation. One popular and

successful approach to derive analytical potential energy surface for molecular dynamics calculations is the semiempirical London–Eyring–Polanyi–Sato (LEPS) potential function and its various extensions,^{22,23} which are based on a valence bond treatment.²⁴ For condensed-phase simulations, a second issue arises, which is the treatment and inclusion of the collective solvent coordinates.⁶ Thus, the PES should be formulated in such a way that it can be conveniently used to represent the solvent reaction coordinate along with the solute reaction path. Although the method that we propose in this paper provides an ab initio valence bond (VB)-like treatment of the PES for polyatomic reactions, our focus in the present study is on the latter aspect, making use of an energy-gap approach to define the solvent reaction coordinate. The energy-gap reaction coordinate has been successfully applied to numerous chemical reactions in the context of empirical valence bond (EVB) calculations.^{25–29} Voth and others have further extended the simple EVB ideas to modeling proton transfer reactions in aqueous systems with multistate EVB configurations.^{30,31} However, one shortcoming in the EVB method is a lack of a systematic path in improving its accuracy, especially when critical experimental data are not readily available. The difficulty may be somewhat alleviated using efficient algorithms for general parametrization from ab initio energy and Hessian results.^{27,32,33} Nevertheless, there is interest in developing a more systematic procedure to treat this problem.

In this article, we present an ab initio approach, suitable for condensed phase simulations, that combines Hartree–Fock molecular orbital theory and modern valence bond theory (MOVB) to describe the PES for reactive systems. The MOVB method is tested in this work on a model proton transfer reaction in water; however, the approach is general and can be applied

* Corresponding author e-mail: gao@chem.umn.edu.

[†] Present address: Department of Chemistry, University of Minnesota, 207 Pleasant Street, SE, Minneapolis, MN 55455.

to any chemical reaction. In what follows, we first review in section 2 a block-localized wave function (BLW) method that is used to define diabatic electronic states. Then the MOVB model is described for computation of the adiabatic PES and its implementation in combined QM/MM simulations. In section 3, computational algorithms are presented for construction of the diabatic electronic state functions for carrying out MOVB free energy simulations and for performing statistical Monte Carlo calculations. This is followed in section 4 by results and discussion of the major findings. Conclusions are given in section 5.

2. Methods

The block-localized wave function (BLW) method was introduced previously and has been applied to organic compounds to rationalize electronic delocalization effects^{34,35} to decompose energy components in intermolecular interactions.³⁵ Here, the BLW method is briefly summarized before the molecular orbital–valence bond approach is described.

A. The Block-Localized Wave Function Method. It is of considerable interest to construct diabatic electronic states representing specific resonance structures of a molecular system. Such diabatic states provide the reference point for computing the electronic delocalization energy in the investigation of intermolecular interactions and chemical bonding.³⁵ Furthermore, the potential energy surface for a chemical reaction can be described by mixing the individual potential energy surfaces for the reactant and product state as well as other important valence bond (VB) configurations.²⁴ An important feature of the VB approach is that it is conceptually closely related to the way in which organic chemists rationalize chemical reactivity, and it has been successfully used by Shaik and co-workers to describe organic reactions.^{36–38} In principle, modern ab initio valence bond theory can be used to construct the localized wave function for specific diabatic states; however, ab initio VB calculations are extremely time consuming, which prevents its application to large molecules of biological interest.

Here, we construct the localized diabatic state, or resonance structure, using a strictly block-localized wave function (BLW) method, which was developed recently for the study of electronic delocalization.^{34,35} This approach is similar, but different in implementation, to ideas that have been developed by Gianinetti et al. for the study of intermolecular interactions.^{39,40} Before we proceed, we note that although it is possible to construct electronic diabatic states using localized molecular orbitals derived from unitary transformation of canonical orbitals,⁴¹ these localized MOs are in fact not strictly localized. They contain both orthogonalization and delocalization tails, the latter of which makes contribution to the electronic delocalization effect and is not appropriate for describing diabatic potential energy surfaces. To avoid these two types of tails in the BLW method, we impose restrictions on the expansion space of the molecular orbitals.³⁵

It turns out that it is always possible to partition all electrons and basis orbitals in a molecular system into k subgroups, corresponding to a particular form of the Lewis resonance or VB structure. For simplicity, we assume that each subgroup is a closed-shell system; the a th subgroup contains m_a basis functions and n_a electrons. The extension of the BLW method to open-shell partitions is straightforward, and the computational details will be described in a forthcoming paper. Thus, the total number of primitive basis functions, M , and the total number of electrons, N , in the system are

$$M = \sum_{a=1}^k m_a \quad \text{and} \quad N = \sum_{a=1}^k n_a \quad (1)$$

Each molecular orbital in a subgroup is written as a linear combination of the primitive basis functions in that specific subspace $\{\chi_\mu^a, \mu = 1, \dots, m_a\}$

$$\varphi_j^a = \sum_{\mu=1}^{m_a} c_{j\mu}^a \chi_\mu^a \quad (2)$$

The Slater determinant wave function for resonance structure s is then constructed as

$$\Psi_s = \hat{A}(\Phi_1 \Phi_2 \dots \Phi_{k_s}) \quad (3)$$

where \hat{A} is an antisymmetrizing operator, Φ_a is a successive product of the occupied MOs in the a th subgroup (eq 2), and k_s is the number of electronic blocks

$$\Phi_a = \varphi_1^a \alpha \varphi_1^a \beta \varphi_2^a \alpha \dots \varphi_{n_a/2}^a \beta \quad (4)$$

where α and β are spin functions. The wave function defined in eq 3 is subjected to the restriction that molecular orbitals within each subgroup are orthogonal, whereas orbitals between different subgroups are nonorthogonal—a feature of the valence bond approach^{42–45}

$$\langle \varphi_i^a | \varphi_j^b \rangle = \begin{cases} \delta_{ij}, & a = b \\ \mathbf{O}_{ij}, & a \neq b \end{cases} \quad (5)$$

where \mathbf{O}_{ij} is the overlap integral between molecular orbital i and j .

With the definition of eqs 2 and 3, the coefficient matrix for the occupied MOs of the BLW wave function has the following form:

$$\mathbf{C}_s = \begin{pmatrix} \mathbf{C}^1 & 0 & \dots & 0 \\ 0 & \mathbf{C}^2 & \dots & 0 \\ \dots & \dots & \dots & \dots \\ 0 & 0 & \dots & \mathbf{C}^{k_s} \end{pmatrix} \quad (6)$$

where the element \mathbf{C}^a is an $n_a/2 \times m_a$ matrix whose elements are defined in eq 2. The energy of the localized wave function (diagonal terms of the Hamiltonian) is determined as the expectation value of the Hamiltonian H , which is given as follows:

$$E_s = \langle \Psi_s | H | \Psi_s \rangle = \sum_{\mu=1}^S \sum_{\nu=1}^S \mathbf{d}_{\mu\nu} \mathbf{h}_{\mu\nu} + \sum_{\mu=1}^S \sum_{\nu=1}^S \mathbf{d}_{\mu\nu} \mathbf{F}_{\mu\nu} \quad (7)$$

In eq 7, $\mathbf{h}_{\mu\nu}$ and $\mathbf{F}_{\mu\nu}$ are, respectively, elements of the usual one-electron and Fock matrices, and $\mathbf{d}_{\mu\nu}$ is an element of the density matrix, \mathbf{D} , which is evaluated using eq 8

$$\mathbf{D} = \mathbf{C}(\mathbf{C}^+ \mathbf{S} \mathbf{C})^{-1} \mathbf{C}^+ \quad (8)$$

where \mathbf{S} is the overlap matrix of primitive basis functions, $\{\chi_\mu^a, \mu = 1, \dots, m_a; a = 1, \dots, k_s\}$.

The molecular orbitals in the BLW wave function can be optimized in two ways using (1) the Jacobi rotation method,³⁴ or (2) a reorthogonalization technique described by Gianinetti et al.³⁹ Both approaches have been implemented in our program. The reorthogonalization method is approximately 10 times faster

than the successive Jacobi rotation algorithm for the system investigated here.

B. The Molecular Orbital–Valence Bond Method. The wave function for a reacting system along the entire reaction coordinate, $\Theta[R,X]$, can be described by the resonance of the reactant Ψ_1 and product Ψ_2 configurations, plus other important configurations if necessary:

$$\Theta[R,X] = \sum_r^L v_r \Psi_r[R,X] \quad (9)$$

where each $\Psi_r[R,X]$ represents a specific diabatic state, $\Theta[R,X]$ is an adiabatic state wave function, L is the total number of diabatic states, and the coefficients $\{v_r\}$ are determined variationally analogous to multiconfiguration self-consistent field (MCSCF) calculations. To emphasize the fact that the diabatic and adiabatic ground state (as well as excited state) wave functions depend on the geometry of the reactive system R and the solute–solvent reaction coordinate X , these variables are explicitly indicated in eq 9. Since the resonance VB-like structures defined by eqs 3 and 9 have features both of molecular orbital theory and modern ab initio VB method, the present approach is referred to as the molecular orbital–valence bond (MOVB) method.

The MOVB Hamiltonian in the basis of the valence bond configurations is constructed by determining the VB integrals and relevant overlap integrals, and the ground state energy is obtained by diagonalizing the Hamiltonian of eq 10

$$H = \begin{pmatrix} H_{11} & H_{12} & \dots & H_{1L} \\ H_{21} & H_{22} & \dots & H_{2L} \\ \dots & \dots & \dots & \dots \\ H_{L1} & H_{L2} & \dots & H_{LL} \end{pmatrix} \quad (10)$$

where L is the total number of diabatic states defined in eq 9, which are also referred to as MOVB configurations. The diagonal matrix element in eq 10 can be conveniently evaluated by using eq 7, which has been applied to the study of resonance effects.³⁵ The off-diagonal element H_{st} is defined as follows:

$$H_{st} = \langle \Psi_s | H | \Psi_t \rangle \quad (11)$$

Evaluation of H_{st} ($s \neq t$) involves two Slater determinants whose spin–orbitals are nonorthogonal. A number of algorithms have been proposed for this problem. Löwdin first described a method on the basis of the Jacobi ratio theorem,⁴⁶ whereas Amos and Hall⁴⁷ and King et al.⁴⁸ developed a bi-orthogonalization procedure for evaluation of matrix elements of nonorthogonal determinant wave functions. In our implementation, we follow Löwdin's Jacobi ratio strategy, which is summarized below.

For convenience of discussion, we rewrite the two BLW functions appearing in eq 11 for the VB configuration s and t as follows:

$$\Psi_s[R,X] = M_s(N!)^{1/2} \det |s_1\alpha(1)s_1\beta(2)\dots s_{N/2}\beta(N)| \quad (12a)$$

$$\Psi_t[R,X] = M_t(N!)^{1/2} \det |t_1\alpha(1)t_1\beta(2)\dots t_{N/2}\beta(N)| \quad (12b)$$

where M_s and M_t are normalization constants, s_i and t_i are spatial orbitals for configuration s and t . Here, we have replaced the notation for molecular orbitals, φ^a_i (eq 2), with the correspondence of $s_1 \leftrightarrow \varphi^1_1$; $s_2 \leftrightarrow \varphi^1_2$, ..., $s_{N/2} \leftrightarrow \varphi^k_{nk/2}$. A similar correspondence for configuration t can also be made. Note that configuration s and t may or may not have the same number of blocks (subgroups) in constructing the BLW wave function,

although the total number of molecular orbitals is identical. Recognizing that the $N \times N$ determinant BLW wave function (eq 12) can be partitioned into two equivalent $N/2 \times N/2$ matrices, one corresponding to the α spin and the other β spin, H_{st} can be conveniently expressed in terms of only spatial orbitals. First, the overlap integral between Ψ_s and Ψ_t is

$$\langle \Psi_s | \Psi_t \rangle = M_s M_t D_{st}^2 \quad (13)$$

where D_{st} is the determinant of the overlap matrix between the spatial molecular orbitals in Ψ_s and Ψ_t

$$S_{st} = \begin{pmatrix} \langle s_1 | t_1 \rangle & \dots & \langle s_1 | t_{N/2} \rangle \\ \dots & \dots & \dots \\ \langle s_{N/2} | t_1 \rangle & \dots & \langle s_{N/2} | t_{N/2} \rangle \end{pmatrix} \quad (14)$$

$$D_{st} = \det |S_{st}| \quad (15)$$

To evaluate H_{st} , we consider the one-electron and two-electron terms of the Hamiltonian separately. The contribution from the one-electron part is

$$\langle \Psi_s | \sum_i h(i) | \Psi_t \rangle = 2M_s M_t D_{st}^2 \sum_{i=1}^{N/2} \sum_{j=1}^{N/2} \langle s_i | h(1) | t_j \rangle (S_{st}^{-1})_{ji} \quad (16)$$

where $(S_{st}^{-1})_{ji}$ is an element of the inverse matrix of S_{st} (eq 14), which can be conveniently derived using the Jacobi ratio theorem⁴⁶

$$(S_{st}^{-1})_{ji} = \frac{D_{st}(s_i t_j)}{D_{st}} \quad (17)$$

where $D_{st}(s_i t_j)$ is the algebraic residual corresponding to the i th column, j th row element of the determinant S_{st} in eq 14. Defining the density matrix \mathbf{P} as

$$P_{\mu\nu} = \sum_{i=1}^{N/2} \sum_{j=1}^{N/2} c_{i\mu}^s c_{j\nu}^t (S_{st}^{-1})_{ji} \quad (18)$$

eq 16 can be simplified in terms of the primitive orbital integrals $h_{\mu\nu}$

$$\langle \Psi_s | \sum_i h(i) | \Psi_t \rangle = 2M_s M_t D_{st}^2 \sum_{\mu\nu} P_{\mu\nu} h_{\mu\nu} \quad (19)$$

Similarly, the two-electron Hamiltonian part yields

$$\left\langle \Psi_s \left| \sum_{i>j} \frac{1}{r_{ij}} \right| \Psi_t \right\rangle = M_s M_t D_{st}^2 \sum_{\mu\nu} \sum_{\lambda\sigma} (2P_{\mu\nu} P_{\lambda\sigma} - P_{\mu\sigma} P_{\lambda\nu}) \langle \mu\nu | \lambda\sigma \rangle \quad (20)$$

Combining eqs 19 and 20, we obtain

$$H_{st} = M_s M_t D_{st}^2 \left[\sum_{\mu\nu} 2P_{\mu\nu} h_{\mu\nu} + \sum_{\mu\nu} \sum_{\lambda\sigma} (2P_{\mu\nu} P_{\lambda\sigma} - P_{\mu\sigma} P_{\lambda\nu}) \langle \mu\nu | \lambda\sigma \rangle \right] \quad (21)$$

It is noted that H_{st} is a function of the geometry and the reaction coordinate of the reacting system, $R(X)$.

C. Combined Ab Initio QM/MM Simulation Techniques. Our main goal is to incorporate solvent effects into ab initio Monte Carlo or molecular dynamics simulations of chemical processes, making use of combined quantum mechanical and molecular mechanical (QM/MM) techniques. QM/MM tech-

niques have been implemented for Hartree–Fock, configuration interaction, and density functional calculations, and they have been applied to a variety of chemical systems with remarkable success. Interested readers may find further computational details in refs 8–12. The present study extends these solvation techniques to the MOVB method for reactive systems.

In a combined QM/MM method, the interaction Hamiltonian between the QM solute and MM solvent is included in the optimization of the solute wave function by incorporating the one-electron integral term resulting from the solvent electric field

$$h_{\mu\nu}^{\text{qm/mm}} = h_{\mu\nu}^{\text{o}} + I_{\mu\nu}^{\text{qm/mm}} \quad (22)$$

where $h_{\mu\nu}^{\text{o}}$ is an element of the usual one-electron matrix for the isolated “QM” system. The one-electron integral $I_{\mu\nu}^{\text{qm/mm}}$ in eq 22 consists of contributions from all solvent charges^{10,11} which can be evaluated using standard algorithms for computing nuclear-attraction integrals. Thus, the MOVB energy automatically includes solute–solvent electrostatic interactions.

3. Computational Details

The present MOVB method for studying chemical reactions in solution is illustrated by computing the potential of mean force for the proton-transfer reaction between ammonium ion and ammonia, $[\text{H}_3\text{N}\cdots\text{H}\cdots\text{NH}_3]^+$, in water.^{49–51} Since the primary goal of the present study is to examine the MOVB method for describing the potential energy surface in a chemical reaction in solution, the nuclear quantum mechanical tunneling effect is not specifically considered. First, we show that the MOVB method yields reasonable results for the ground state PES of the proton transfer reaction both in the gas phase and in solution. Second, we illustrate that the diabatic PES of the MOVB method can be effectively used as a mapping potential in potential of mean force calculations.

A. The MOVB Potential Energy for the Proton Transfer Reaction in $[\text{H}_3\text{N}\cdots\text{H}\cdots\text{NH}_3]^+$. We use three resonance configurations to describe the proton transfer reaction in $[\text{H}_3\text{N}\cdots\text{H}\cdots\text{NH}_3]^+$

$$\begin{aligned} \Psi_3 &= \{\text{H}_3\text{N}:\text{H}^+:\text{NH}_3\} = \hat{A}[\Phi(\text{H}_3\text{N})\Phi(\text{NH}_3)] \\ \Psi_2 &= \{\text{H}_3\text{N}:\text{H}-\text{NH}_3^+\} = \hat{A}[\Phi(\text{H}_3\text{N})\Phi(\text{H}-\text{NH}_3^+)] \quad (23) \\ \Psi_1 &= \{\text{H}_3\text{N}-\text{H}^+:\text{NH}_3\} = \hat{A}[\Phi(\text{H}_3\text{N}-\text{H}^+)\Phi(\text{NH}_3)] \end{aligned}$$

where each Φ indicates a product of the molecular orbitals expanded over basis functions located on atoms in the fragment specified in parentheses. These MOs are optimized for each resonance structure using the method described in refs 34 and 39 at a given geometry of the molecule. Although the MO coefficients for each resonance configuration may in principle be optimized in the MOVB CI calculations, only the configuration coefficients are variationally optimized here. The ground state energy is obtained by diagonalizing the three-state MOVB Hamiltonian (eq 10). For comparison, the proton transfer potential energy curve is also computed at the Hartree–Fock level.

The diabatic potential energy for each resonance configuration as well as the adiabatic ground state energy for the reaction in solution is determined by including the solute–solvent (or qm/mm) one-electron integrals, $I_{\mu\nu}^{\text{qm/mm}}$, in the gas phase one-electron matrix. Thus, both the diagonal, H_{ss} , and off-diagonal, H_{st} , matrix element in the MOVB Hamiltonian explicitly include solvent effects in the calculation. This is in contrast to Warshel’s

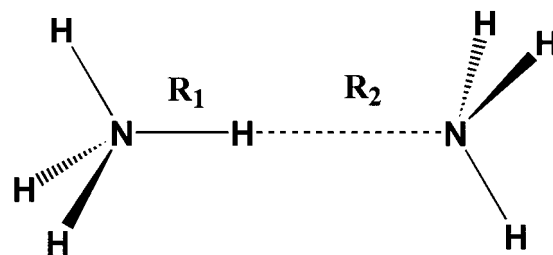


Figure 1. Schematic representation of the geometrical parameters for the $[\text{H}_3\text{N}-\text{H}-\text{NH}_3]^+$ system.

EVB approach,^{25,26} in which the solvent contribution is incorporated only into the diagonal elements, whereas the off-diagonal elements are assumed to be independent of solvent effects. Although the most significant contribution to the variation in off-diagonal matrix elements is their dependence on the solute geometry, it has been pointed out that in many cases, the solvent dependence of the off-diagonal matrix elements is not negligible in studying chemical reactions in solution using a VB approach.^{28,30} Since our ab initio MOVB method includes these contributions explicitly in all terms, it provides a means by which this problem can be assessed in condensed phase simulations by comparison with studies that exclude the solvation term in H_{st} . This study will be reported in a future publication.

In this work, we have used the 3-21G basis set to demonstrate the method in liquid simulations, while larger basis functions are used for gas phase comparisons.

B. Free Energy Perturbation Methods. The potential of mean force, or free energy profile, as a function of the reaction coordinate, X , for a chemical reaction in solution can be computed using the free energy perturbation method.⁵² A straightforward approach is to determine free energy differences for incremental changes of certain geometrical variables that characteristically reflect the chemical process in going from the reactants, through the transition state, to the final products.⁵³ For example, X may be defined by some characteristic geometry variables, specifying the position of the migrating proton in $[\text{H}_3\text{N}\cdots\text{H}\cdots\text{NH}_3]^+$, $X^{\text{R}} = R_1 - R_2$ (Figure 1). Here, we use the superscript R to stress the fact that the reaction coordinate is defined by the solute geometrical parameters. The potential of mean force is then determined using the free energy perturbation theory⁵²

$$\Delta G(X_n^{\text{R}}) = -RT \sum_{j=1}^n \ln \langle e^{-[E(X_j^{\text{R}}) - E(X_{j-1}^{\text{R}})]/RT} \rangle_{j-1} \quad (24)$$

where the brackets $\langle \dots \rangle_j$ indicate an ensemble average over the potential energy $E(X_j^{\text{R}})$, and n is the number of “bins” (increments) in going from the reactant state (X_0^{R}) to a value of X_n^{R} . This “geometric mapping” approach, which is akin to studying gas phase reactions through reaction path calculations, has been successfully applied to numerous organic reactions in solution.⁵⁴ Nevertheless, there is concern in this type of simulations because the solvent reaction coordinate is not explicitly included in the definition of the reaction coordinate.⁵⁵ A recent simulation study of the proton transfer in $[\text{HO}\cdots\text{H}\cdots\text{OH}]^-$ in water indicates that there is considerable difference in the qualitative appearance of the free energy profile and the height of the predicted free energy barrier if the solvent reaction coordinate is explicitly taken into account.⁵⁵

An alternative approach for obtaining the activation barrier and the free energy reaction profile is to define X in such a way as to reflect both the solute and solvent reaction coordinate.⁶

Therefore, if X is chosen as the energy difference between the energies of the diabatic reactant and product VB states in solution, the solvent degrees of freedom are adequately defined because the change in solute–solvent interaction energy reflects the collective motions of the solvent molecules as the reaction proceeds^{6,26,55}

$$X^S = E_1(\Psi_1) - E_2(\Psi_2) \quad (25)$$

where E_1 and E_2 are the expectation values of the wave functions Ψ_1 and Ψ_2 , defined in eq 23, and the superscript S emphasizes explicit treatment of the solvent reaction coordinate. It should be noted that X^S is negative when the system is in the reactant state and positive in the product state. Although eq 25 is not unique in defining the solvent reaction coordinate, it provides a convenient procedure to monitor the progress of the reaction in solution.

In practice, a reference potential (RP), or mapping potential, must be used to enforce the orientation polarization of the solvent system such that significant time is spent along the entire reaction path, particularly at the transition state region. One approach that has been successfully used previously is to linearly couple the reactant and product VB potential energies shown in eq 26:

$$E_{RP}(\lambda) = (1 - \lambda)E_1(\Psi_1) + \lambda E_2(\Psi_2) \quad (26)$$

By moving the coupling variable λ from 0 to 1, the system is driven accordingly from the reactant state $E_1(\Psi_1)$ to the product state $E_2(\Psi_2)$. The free energy change along this RP path can be determined by using eq 24, except that the perturbation is made with respect to small increments in λ , typically at intervals of ± 0.1 .

However, the reference potential (eq 26) is used only to drive the system to go from configurations corresponding to the reactant state to the final product state. To obtain the true ground state potential of mean force, an umbrella sampling procedure is applied to sample the probability of finding configurations at a given value of X^S

$$\Delta G(X^S) = \Delta G_{RP}(\lambda) - RT \ln \langle e^{-[E_g - E_{RP}(\lambda)]/RT} \rangle_\lambda - RT \ln \rho[X^S(\lambda)] \quad (27)$$

where $\Delta G_{RP}(\lambda)$ is the free energy change on the reference potential from 0 to λ , and the average is determined using the potential, $E_{RP}(\lambda)$. The quantity $\rho[X^S(\lambda)]$ in eq 27 is the normalized distribution of configuration that has a value of X^S during the simulation using the reference potential. It should be noted that the umbrella sampling calculation is performed, on the fly, using the same set of Monte Carlo or molecular dynamics trajectories in the free energy perturbation calculation.

In eq 27, the ground state potential E_g can be either the MOVb adiabatic potential energy or any other ab initio quantum mechanical energies, e.g., the HF, MP2, or DFT values. Consequently, the present method is not limited to the MOVb potential energy surface. In the present study, we choose to use both the MOVb and the Hartree–Fock energy as the ground state potential to compare the performance of the method.

The simulation procedure described above has been effectively utilized by Warshel and others to study chemical reactions in solution and in enzymes.^{26,29,30} In these calculations, the EVB method is typically used to describe the VB resonance structure, in which the empirical potential parameters are calibrated to reproduce experimental data, and the empirical force field makes it convenient to describe the diabatic VB states in

solution. It is, however, difficult to use this approach directly in ab initio QM/MM calculations due to complications in constructing diabatic VB states.⁵⁵ The present MOVb method provides the first practical procedure to directly include the solvent reaction coordinate in combined ab initio QM/MM simulation of chemical reactions in solution.

C. Monte Carlo Simulations. Statistical mechanical Monte Carlo simulations have been carried out for systems consisting of the ammonium–ammonia pair plus 510 water molecules in a cubic cell with periodic boundary conditions. Standard procedures were used, including Metropolis sampling and the isothermal–isobaric ensemble (NPT) at 25 °C and 1 atm. To facilitate the statistics near the solute molecule, the Owicki–Schraga preferential sampling technique was adopted with $1/(r^2 + C)$ weighting, where $C = 150 \text{ \AA}^2$. The intermolecular interactions were feathered to zero at a spherical cutoff distance between 9.5 and 10 Å based on heavy atom separations. New configurations were generated by randomly selecting a molecule, translating it in all three Cartesian directions, and rotating it around a randomly chosen axis. For solute moves, all internal geometric parameters including bond lengths, bond angles, and dihedral angles are varied, except that the N–H–N atoms are restricted to being linear with a fixed N–N separation of 2.7 Å, which is slightly longer than the equilibrium distance for the ammonium–ammonia complex (2.64 Å). The dynamics and the actual proton transfer pathway are not fully explored here.^{49,50} All simulations were maintained with an acceptance rate of ca. 45% by using ranges of $\pm 0.15 \text{ \AA}$ and 15° for translation and rotation moves of both the solute and solvent molecules. For the internal degrees of freedom for $[\text{H}_3\text{N}\cdots\text{H}\cdots\text{NH}_3]^+$, the N–H bond distances are restricted to be $\pm 0.002 \text{ \AA}$, the H–N–N angles are 5° , and the maximum allowed change in the H–N–N–H dihedral angle is 15° . The range of the central proton has a translation range of 0.03 Å.

The solute $[\text{H}_3\text{N}\cdots\text{H}\cdots\text{NH}_3]^+$ is represented quantum mechanically at the HF and the MOVb level, the latter of which is used to construct the diabatic VB configurations. The three point charge TIP3P model is adopted for water.⁵⁶ QM/MM interactions are incorporated into QM calculations via the one-electron integral term augmented by a nonelectrostatic van der Waals term. The Lennard–Jones parameters for solute atoms are taken from ref 57, which are developed for HF/3-21G QM/MM calculations. The MOVb method has been implemented into the MCQUB program package, with which combined QM/MM Monte Carlo simulations can be carried out both at the semiempirical level and the ab initio level,⁵⁸ using the GAMESS programs for the latter calculation.⁵⁹ The MOVb calculations were performed using a program developed in our group, which makes use of the integral routines in the GAMESS code.⁶⁰

Two sets of simulations were performed at the QM/MM MOVb and HF level, respectively. In the first calculation, the MOVb diabatic states are used to define the solvent reaction coordinate for the proton transfer reaction in water, and the ground state potential of mean force is determined both at the MOVb and HF level. Then, the standard HF–QM/MM geometric mapping procedure was used in a second set of simulations to obtain the potential of mean force as a function of the solute reaction coordinate. Five free energy perturbation windows are used in the MOVb QM/MM calculation, which are more than sufficient in the present calculation, although it allows comparison of the convergence from different starting conditions. In the HF–QM/MM calculation, we used a standard umbrella sampling method to determine the potential of mean force.⁶¹ Two simulations are deemed to be adequate. Each

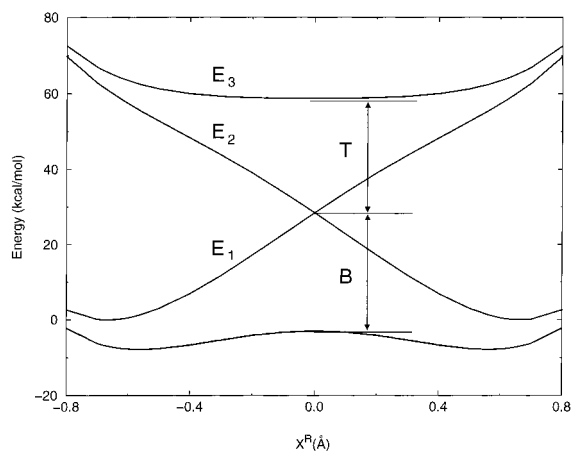


Figure 2. Computed potential energy functions for the diabatic and adiabatic state in the $[\text{H}_3\text{N}-\text{H}-\text{NH}_3]^+$ system in the gas phase using the 6-31G(d) basis function. The reaction profile at the HF/6-31G(d) level is shown in dotted curve, which nearly coincides with the MOVB adiabatic potential energy.

calculation window consisted of at least 2×10^6 configurations of equilibration, followed by 2×10^6 configurations of averaging. All computations are performed on an Origin 2000 computer at the Center for Computational Research at Buffalo.

4. Results and Discussion

A. Gas Phase Potential Energy Surfaces. The diabatic and MOVB adiabatic potential energy profiles for the proton transfer reaction of $\text{NH}_4^+ + \text{NH}_3 \rightarrow \text{NH}_3 + \text{NH}_4^+$ in the gas phase are depicted in Figure 2. The geometries used in the MOVB calculations are taken from the corresponding HF optimization with fixed values of the reaction coordinate X^R , which is defined as the difference between the two H–N bond distances (Figure 1). Furthermore, the N–N distance is fixed at a separation of 2.7 Å, which is used in subsequent simulation calculations.

The potential energy profiles for the two diabatic VB configurations intersect at $X^R = 0$ Å, corresponding to the transition structure where the proton is located in the middle between the two nitrogen atoms (Figure 2). The energy at the crossing point of the two diabatic states, E_1 and E_2 , is 19.4 kcal/mol above the minimum configuration ($X^R = \pm 0.65$ Å) using the 3-21G basis set, and 28.4 and 26.4 kcal/mol, respectively, using the 6-31G(d) and cc-pVTZ basis set. Figure 2 depicts the results obtained using the 6-31G(d) basis set. As expected, the diabatic potential energy surface for the reactant state (E_1) monotonically increases as the proton migrates to the product state. Concomitantly, the potential energy for the product state (E_2) mirrors the change of the reactant state in decreasing order. The potential energy surface for the ionic state, $\Psi_3 = [\text{H}_3\text{N}; \text{H}^+, \cdot\text{NH}_3]$, has a minimum at $X^R = 0$ Å, with an energy $T = 36.1$, 30.4, and 26.9 kcal/mol above the intersection from the three basis sets.

The adiabatic MOVB ground state potential surface is significantly lower in energy than the diabatic surfaces, with a coupling energy of $B = 30.8$, 30.2, and 28.3 kcal/mol at the transition state at the MOVB(3)/3-21G, 6-31G(d), and cc-pVTZ level, respectively (Table 1). The barrier for the proton transfer is predicted to be 1.2 kcal/mol at the MOVB(3)/3-21G level, which may be compared with the Hartree–Fock value of 1.1 kcal/mol using the 3-21G basis set. In this notation, MOVB-(3)/3-21G, the number in parentheses specifies the number of configurations employed in the MOVB calculation. It should be noted that the central proton is more localized toward one

TABLE 1: Computed Activation Energies (kcal/mol) at the HF and MOVB Level and the Adiabatic Coupling B and the Ionic State Energy T (kcal/mol)

basis	$\Delta E_{\text{HF}}^\ddagger$	$\Delta E_{\text{MOVB}}^\ddagger$	B	T
3-21G	1.07	1.18	30.8	36.1
6-31G(d)	4.82	4.91	30.2	30.4
cc-pVTZ	4.64	5.10	28.3	26.9

of the nitrogen atoms in the minimum energy configurations for the diabatic states with a value of $X^R = \pm 0.65$ Å, whereas the minimum configuration on adiabatic potential surface is located at $X^R = 0.55$ Å. The barrier heights predicted using the larger basis sets are substantially greater than the 3-21G value, although the agreement between HF and MOVB results is good (Table 1). This difference is due to the use of a fixed N–N distance of 2.7 Å in these calculations, which is longer than the minimum value at the HF/3-21G level (2.64 Å) but shorter than the HF/6-31G(d) and HF/cc-pVTZ values (2.82 and 2.81 Å). The inner side of the potential energy surface is much steeper than the exterior.⁴⁹ The agreement between MOVB and HF results demonstrates that given a basis set, the MOVB method is reasonable in describing the potential energy surface for a chemical process involving the breaking and formation of chemical bonds. Interestingly, the predicted coupling energy B is relatively insensitive to the basis functions used, whereas the ionic state is significantly stabilized using a large basis set (Table 1).

We note that the representation of the VB resonance structures in the MOVB method makes use of a HF description for the N–H bond in 1 and 2 (eq 23). These configurations can also be described by two covalent VB structures in a way analogous to the GVB approach.⁶² If such a GVB alternative is used to describe the bonding electron pairs, electron correlation effects can be included in MOVB calculations.

B. Bimolecular Complexes. To assess the validity of the MOVB–QM/MM model for simulation of solvent effects on the proton transfer process in water, hydrogen-bonding complexes of $\text{H}_3\text{NH}^+ \cdots \text{NH}_3$ with water have been investigated. The results are compared with HF/3-21G QM/MM calculations and full ab initio HF/6-31G(d) calculations. Intermolecular geometry optimizations for the hybrid potentials are executed using a simulated annealing technique in Monte Carlo calculations, with which the temperature is gradually annealed from 25 °C to –273.0 °C. For the MOVB QM/MM optimization, interaction energies are computed both for the diabatic valence bond configurations and for the adiabatic MOVB ground state potential. In these computations, the $\text{H}_3\text{NH}^+ \cdots \text{NH}_3$ structure is fixed in the geometry at the HF/3-21G level, while experimental values are adopted for water.

Computed interaction energies for the interaction between $[\text{H}_3\text{N} \cdots \text{H} \cdots \text{NH}_3]^+$ and a water molecule are listed in Table 2. Full ab initio HF/6-31G(d) results are compared with data obtained from the hybrid methods at the HF and MOVB levels. The estimated binding energies from QM–HF/3-21G/MM calculations are about 3 kcal/mol smaller than the corresponding full HF/6-31G(d) optimizations. This is a consequence of the relatively longer hydrogen-bond distance predicted at the hybrid level. Although the deviation may be alleviated by adjusting the Lennard–Jones parameters, this optimization was not carried out further because the relative interaction energy on going from the ground state to the transition state structure for $[\text{H}_3\text{N} \cdots \text{H} \cdots \text{NH}_3]^+$ is in reasonable agreement with full ab initio calculations. The MOVB interaction energies follow similar trends as that for the HF/3-21G/TIP3P model, though they are in slightly better accord with the ab initio results. Overall, combined

TABLE 2: Combined Bimolecular Interaction Energies (kcal/mol) for $[\text{H}_3\text{N}\cdots\text{H}\cdots\text{NH}_3]^+$ and Water Complexes

	$\text{H}_2\text{O}\cdots[\text{H}_3\text{N}-\text{H}^+\cdots\text{NH}_3]^a$		$\text{H}_2\text{O}\cdots[\text{H}_3\text{N}\cdots\text{H}\cdots\text{NH}_3]^+a$	
	$R(\text{O}-\text{N}), \text{\AA}$	ΔE	$R(\text{O}-\text{N}), \text{\AA}$	ΔE
HF/6-31G(d)	1.86	-16.1	1.96	-13.2
HF/3-21G-MM	1.91	-13.2	1.95	-11.1
MOVB/3-21G-MM	1.88	-13.3	1.95	-11.1
MOVB(E_1)/3-21G-MM	1.86	-14.2	1.95	-12.6

^a Species in square brackets are treated quantum mechanically in QM/MM calculations using the 3-21G basis set.

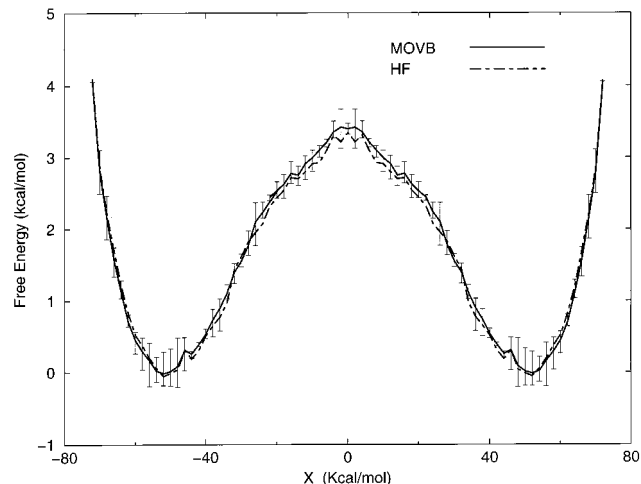


Figure 3. Computed potentials of mean force using the HF/3-21G and MOVB(3)/3-21G ground state potential energy surface from ab initio MOVB/MM Monte Carlo simulations. The N–N distance was fixed at 2.7 Å in all simulations.

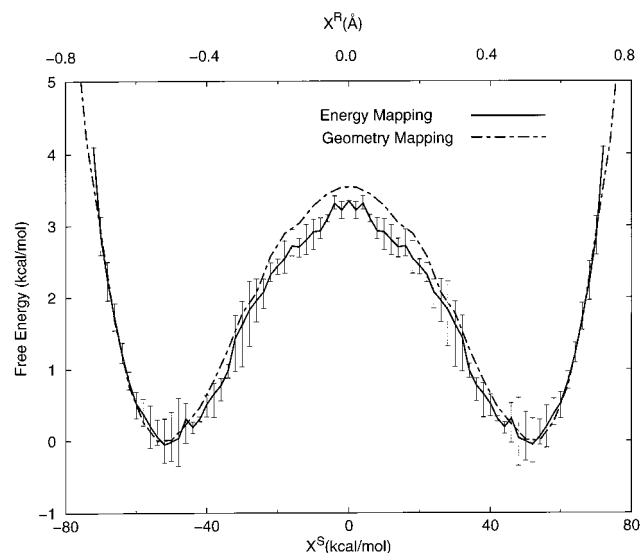


Figure 4. Comparison of computed potentials of mean force from energy mapping (X^S , solid curves) and geometrical mapping (X^R , dash curves) procedures at the HF/3-21G level. The N–N distance was fixed at 2.7 Å in all simulations. The two reaction coordinates are matched by scaling the ground state and transition state positions.

MOVB/MM calculations yield results similar to those from the combined HF/MM model.

C. Potential of Mean Force in Aqueous Solution. Figures 3 and 4 show the key findings of the present study, which illustrate the potential of mean force (pmf) for the proton transfer reaction in aqueous solution. In Figure 3, the free energy changes were obtained as a function of the reaction coordinate $X^S = E_1 - E_2$, using the HF and MOVB ground state potential energy surface. For comparison, the potential of mean force was also determined using a geometrical mapping procedure at the

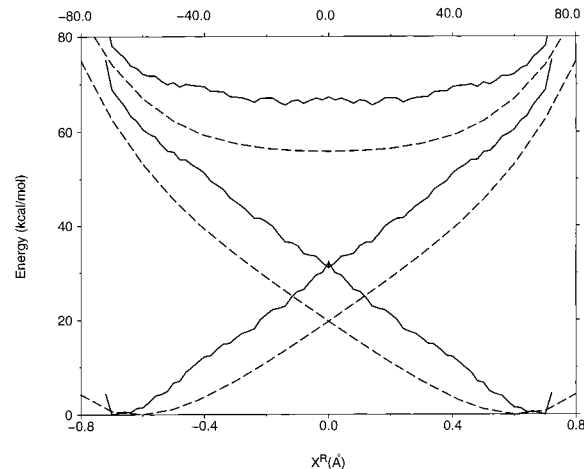


Figure 5. Computed diabatic state potential energy curves, averaged over 2 million configurations, in aqueous solution (solid) and in the gas phase (dashed). The 3-21G basis set is used.

combined HF/3-21G/TIP3P level (Figure 4, dashed curve). Figure 5 depicts the diabatic potential energy surfaces using the 3-21G basis set for the three VB states in the gas phase and in water.

The effect of solvation on the predicted barrier height is significant from both HF and MOVB pmf's in Figures 3. Importantly, the HF and MOVB results are in excellent agreement. At the HF level, the computed activation free energy ΔG^\ddagger is 3.3 kcal/mol, representing an increase of 2.2 kcal/mol over the gas phase process. Similarly, the MOVB activation energy is determined to be 3.4 kcal/mol, in good accord with the HF prediction. The error ranges shown in Figure 3 are estimated from 3 to 5 overlapping windows used in the free energy simulation, which are about ± 0.1 to ± 0.5 kcal/mol. For comparison, large solvent effects on the activation barrier for the proton transfer between NH_4^+ and NH_3 in water have been found previously.^{49,51} Chuang et al. described a method that incorporates a continuum solvation model in electronic structure and dynamics calculations for reactions in solution by making the separable equilibrium solvation and the equilibrium solvation path approximation.⁵¹ Applying this method to the $\text{NH}_4^+\cdots\text{NH}_3$ proton transfer reaction using the PM3 semiempirical model coupled with the SM5.4 solvation model, Chuang et al. found that solvation increases the barrier along the adiabatic potential surface by 4.2 kcal/mol.⁵¹ In this case, the PM3 model significantly overestimates the gas phase reaction barrier in the gas phase, which is 9.5 kcal/mol. Interestingly, it was found that quantum mechanical tunneling is dominated by the large-curvature mechanism.⁵¹ In a separate combined QM/MM AM1/TIP3P Monte Carlo simulation study, the barrier height was estimated to increase by about 2.5 kcal/mol at an N–N separation of 2.7 Å.⁴⁹ The present results suggests that the MOVB method may be effectively utilized to describe the potential energy surface for chemical processes in solution.

It is of interest to compare the predicted activation energy obtained by the geometrical mapping procedure in Monte Carlo

simulations at the combined QM-MM HF/3-21G-TIP3P level. In this case, the solvent reaction coordinate is not explicitly included in the definition of the reaction coordinate, X^R . It should be noted that if the simulation is carried out sufficiently long, the computed barrier heights from these two simulation protocols should be the same. In practice, localization of electronic wave function in combined QM/MM calculations may render difficulties of fast convergence near the transition state region. In the present case of $[\text{H}_3\text{N}-\text{H}-\text{NH}_3]^+$ in water, we found that the predicted ΔG^\ddagger is 3.5 kcal/mol using the geometrical mapping procedure. This is only slightly greater than that obtained using X^S as the reaction coordinate (3.3 kcal/mol). The present finding is in contrast to a recent study of the proton transfer of $[\text{HO}\cdots\text{H}\cdots\text{OH}]^-$ system, where significant difference in the predicted activation barrier was found between the geometrical and energy mapping procedures.⁵⁵ In that case, the overall barrier height (20 kcal/mol) is much greater than that of the present system, which results in greater dependence of the computed reaction profile on the solvent reaction coordinate.⁵⁵

Solvation effects on the potential energy surface of the individual diabatic states are shown in Figure 5. As expected, the E_1 and E_2 diabatic states are more stabilized in the ground state region than at the transition state by solvation because charges are more delocalized in the latter state. At $X^S = 0$ kcal/mol, the solvent effect raises the diabatic state energy by ca. 13 kcal/mol over the gas phase value ($X^R = 0$ Å). A similar energy increase is obtained for the ionic state across the entire range of the reaction coordinate. Interestingly, the predicted activation energy in aqueous solution exhibits a rather small solvent effect of 2.2 kcal/mol (Figure 3), although the individual diabatic states consist of much greater increase in energy as the reaction proceeds from the ground (or product) state to the transition state. This shows a remarkable coupling effect of the VB resonance structures. The agreement between HF and MOVB free energies supports the validity of the MOVB method in describing the ground state potential energy surface in solution.

5. Conclusions

We have described a mixed molecular orbital and valence bond (MOVB) model for describing the potential energy surface of reactive systems and presented an application of the method to a model proton transfer reaction in aqueous solution to demonstrate its feasibility in combined ab initio QM/MM simulations. The MOVB model is based on the block-localized wave function (BLW) method, which is used to define the diabatic electronic state functions. A configuration interaction Hamiltonian is constructed using these diabatic VB state as the basis functions. We have presented results showing the change of the diabatic potential energy surface as a function of the proton coordinate in the gas phase, and found a strong electronic coupling energy of $B = 30$ kcal/mol. The ionic state has a minimum, located at a geometry corresponding to the transition state on the ground state adiabatic potential energy surface. This minimum is about 27–36 kcal/mol higher in energy than the crossing point of the two covalent diabatic states. Solvent effects are incorporated into the MOVB Hamiltonian in the spirit of combined QM/MM calculations and have been modeled in Monte Carlo simulations for the proton transfer between ammonium ion and ammonia in water. The potentials of mean force are computed via free energy perturbation coupled with umbrella sampling techniques using (1) an energy mapping approach, and (2) a geometrical mapping procedure. Solvent

effects increase the barrier height by about 2.2 kcal/mol from both the MOVB and the HF ground state potential energy surface. The diabatic states are more stabilized by aqueous solvation in the ground state region than at the transition state. The present study demonstrated the feasibility of ab initio MOVB, albeit using a modest basis function in the present investigation, for studying chemical reactions that incorporate explicitly the solvent reaction coordinate in combined ab initio QM/MM simulations.

Acknowledgment. This work has been generously supported by the National Institutes of Health and the National Science Foundation. We thank Professor Donald G. Truhlar for carefully reading the manuscript and numerous suggestions.

References and Notes

- Truhlar, D. G.; Kuppermann, A. *J. Am. Chem. Soc.* **1971**, *93*, 1840.
- Fukui, K. *Acc. Chem. Res.* **1981**, *14*, 363–836.
- Miller, W. H.; Handy, N. C.; Adams, J. E. *J. Chem. Phys.* **1980**, *72*, 99–112.
- Hehre, W. J.; Radom, L.; Schleyer, P. v. R.; Pople, J. A. *Ab Initio Molecular Orbital Theory*; John Wiley & Sons: New York, 1986.
- Heidrich, D. *The Reaction Path in Chemistry*; Kluwer: Dordrecht, The Netherlands, 1995; Vol. 16.
- Warshel, A. *Computer Modeling of Chemical Reactions in Enzymes and Solutions*; Wiley: New York, 1991.
- Truhlar, D. G.; Hase, W. L.; Hynes, J. T. *J. Phys. Chem.* **1983**, *87*, 2664–2682.
- Warshel, A.; Levitt, M. *J. Mol. Biol.* **1976**, *103*, 227–249.
- Singh, U. C.; Kollman, P. A. *J. Comput. Chem.* **1986**, *7*, 718–730.
- Field, M. J.; Bash, P. A.; Karplus, M. *J. Comput. Chem.* **1990**, *11*, 700.
- Gao, J.; Xia, X. *Science* **1992**, *258*, 631–635.
- Gao, J. *Acc. Chem. Res.* **1996**, *29*, 298–305.
- Gao, J.; Thompson, M. A. *Combined Quantum Mechanical and Molecular Mechanical Methods*; American Chemical Society: Washington, DC, 1998; Vol. 712.
- Gao, J.; Furlani, T. R. *IEEE Comput. Sci. Eng.* **1995**, 24–33.
- Alhambra, C.; Wu, L.; Zhang, Z.-Y.; Gao, J. *J. Am. Chem. Soc.* **1998**, *120*, 3858–3866.
- Hartsough, D. S.; Merz, K. M., Jr. *J. Phys. Chem.* **1995**, *99*, 384–390.
- Merz, K. M., Jr.; Banci, L. *J. Phys. Chem.* **1996**, *100*, 17414–17420.
- Assfeld, X.; Ferre, N.; Rivail, J.-L. *ACS Symp. Ser.* **1998**, *712*, 234–249.
- Liu, H.; Mueller-Plathe, F.; van Gunsteren, W. F. *J. Mol. Biol.* **1996**, *261*, 454–469.
- Chatfield, D. C.; Brooks, B. R. *J. Am. Chem. Soc.* **1995**, *117*, 5561–5572.
- Alhambra, C.; Gao, J.; Corchado, J. C.; Villa, J.; Truhlar, D. G. *J. Am. Chem. Soc.* **1999**, *121*, 2253–2258.
- Eyring, H.; Polanyi, M. *Naturwissenschaften* **1930**, *18*, 914.
- Sato, S. *Bull. Chem. Soc. Jpn.* **1955**, *28*, 450.
- London, F. Z. *Elektrochem.* **1929**, *35*, 551.
- Warshel, A.; Weiss, R. M. *J. Am. Chem. Soc.* **1980**, *102*, 6218–6226.
- Aaqvist, J.; Warshel, A. *Chem. Rev.* **1993**, *93*, 2523–2544.
- Chang, Y. T.; Miller, W. H. *J. Phys. Chem.* **1990**, *94*, 5884–5888.
- Kim, H. J.; Hynes, J. T. *J. Chem. Phys.* **1990**, *93*, 5211–5223.
- Hinsen, K.; Roux, B. *J. Chem. Phys.* **1997**, *106*, 3567–3577.
- Schmitt, U. W.; Voth, G. A. *J. Phys. Chem. B* **1998**, *102*, 5547–5551.
- Vuilleumier, R.; Borgis, D. *Chem. Phys. Lett.* **1998**, *284*, 71–77.
- Chang, Y.-T.; Minichino, C.; Miller, W. H. *J. Chem. Phys.* **1992**, *96*, 4341.
- Kim, Y.; Corchado, J. C.; Villa, J.; Xing, J.; Truhlar, D. G. *J. Chem. Phys.* **2000**, *112*, 0000.
- Mo, Y.; Peyerimhoff, S. D. *J. Chem. Phys.* **1998**, *109*, 1687–1697.
- (a) Mo, Y.; Zhang, Y.; Gao, J. *J. Am. Chem. Soc.* **1999**, *121*, 5737–5742. (b) Mo, Y.; Gao, J. *J. Chem. Phys.* **2000**, in press.
- Pross, A.; Shaik, S. S. *Acc. Chem. Res.* **1983**, *16*, 363–370.
- Shaik, S. S.; Pross, A. *J. Am. Chem. Soc.* **1982**, *104*, 2708–2719.
- Lauvergnat, D.; Hiberty, P. C.; Danovich, D.; Shaik, S. *J. Phys. Chem.* **1996**, *100*, 5715–5720.
- Gianinetti, E.; Raimondi, M.; Tornaghi, E. *Int. J. Quantum Chem.* **1996**, *60*, 157.

- (40) Raimondi, M.; Gianinetti, E. *J. Phys. Chem.* **1988**, *92*, 899–903.
- (41) Glendening, E. D.; Weinhold, F. *J. Comput. Chem.* **1998**, *19*, 593–609.
- (42) Gerratt, J.; Cooper, D. L.; Karadakov, P. B.; Raimondi, M. *Chem. Soc. Rev.* **1997**, *26*, 87–100.
- (43) Cooper, D. L.; Gerratt, J.; Raimondi, M. *Chem. Rev.* **1991**, *91*, 929–964.
- (44) McWeeny, R. *Pure Appl. Chem.* **1989**, *61*, 2087–2101.
- (45) Cooper, D. L.; Gerratt, J.; Raimondi, M. *Adv. Chem. Phys.* **1987**, *69*, 319–397.
- (46) Löwdin, P.-O. *Phys. Rev.* **1955**, *97*, 1474.
- (47) Amos, A. T.; Hall, G. G. *Proc. R. Soc. London* **1961**, *Ser. A263*, 482.
- (48) King, H. F.; Staton, R. E.; Kim, H.; Wyatt, R. E.; Parr, R. G. *J. Chem. Phys.* **1967**, *47*, 1936.
- (49) Gao, J. *Int. J. Quantum Chem.: Quantum Chem. Symp.* **1993**, *27*, 491–499.
- (50) Jaroszewski, L.; Lesyng, B.; Tanner, J. J.; McCammon, J. A. *Chem. Phys. Lett.* **1990**, *175*, 282.
- (51) Chuang, Y.-Y.; Cramer, C. J.; Truhlar, D. G. *Int. J. Quantum Chem.* **1998**, *70*, 887–896.
- (52) Zwanzig, R. *J. Chem. Phys.* **1961**, *34*, 1931–1935.
- (53) Chandrasekhar, J.; Smith, S. F.; Jorgensen, W. L. *J. Am. Chem. Soc.* **1984**, *106*, 3049–350.
- (54) Jorgensen, W. L.; Blake, J. F.; Madura, J. D.; Wierschke, S. D. *ACS Symp. Ser.* **1987**, *353*, 200–17.
- (55) Muller, R. P.; Warshel, A. *J. Phys. Chem.* **1995**, *99*, 17516–17524.
- (56) Jorgensen, W. L.; Chandrasekhar, J.; Madura, J. D.; Impey, R. W.; Klein, M. L. *J. Chem. Phys.* **1983**, *79*, 926–935.
- (57) Freindorf, M.; Gao, J. *J. Comput. Chem.* **1996**, *17*, 386–395.
- (58) Gao, J. *MCQUB*; 3.0 ed.: SUNY, Buffalo, NY, 1998.
- (59) Schmidt, M. W.; Baldrige, K. K.; Boatz, J. A.; Elbert, S. T.; Gordon, M. S.; Jensen, J. H.; Koseki, S.; Matsunaga, N.; Nguyen, K. A.; Su, S. J.; Windus, T. L.; Dupuis, M.; Montgomery, J. S. *GAMESS*; 11 ed., 1993.
- (60) Mo, Y.; Gao, J. *MOVB: A program for calculating diabatic and adiabatic state energies.*; Version 0.2; SUNY, Buffalo: Buffalo, New York, 1999.
- (61) Valleau, J. P.; Torrie, G. M. *A guide to Monte Carlo for statistical mechanics: 1. Highways.*; Berne, B. J., Ed.; Plenum: New York, 1977; Vol. 5, p 169.
- (62) Goddard, W. A., III.; Dunning, T. H., Jr.; Hunt, W. J.; Hay, P. J. *Acc. Chem. Res.* **1973**, *6*, 368–376.